ELSEVIER

Marine Geology 225 (2006) 311–330

MARINE GEOLOGY
INTERNATIONAL JOURNAL OF MARINE GEOLOGY, GEOCHEMISTRY AND GEOPHYSICS

www.elsevier.com/locate/margeo

# The generating mechanisms of the August 17, 1999 İzmit bay (Turkey) tsunami: Regional (tectonic) and local (mass instabilities) causes

Stefano Tinti [a,*], Alberto Armigliato [a], Anna Manucci [a], Gianluca Pagnoni [a], Filippo Zaniboni [a], Ahmet Cevdet Yalçiner [b], Yildiz Altinok [c]

[a] *Università di Bologna, Dipartimento di Fisica, Settore di Geofisica, Viale Carlo Berti Pichat, 8, 40127 Bologna, Italy*
[b] *Middle East Technical University, Department of Civil Engineering, Ocean Engineering Research Center, 06531, Ankara, Turkey*
[c] *Istanbul University, Department of Geophysical Engineering, Division of Seismology, 34850, Avcilar, Istanbul, Turkey*

Received 23 November 2004; received in revised form 22 August 2005; accepted 2 September 2005

**Abstract**

The $M_W = 7.4$ earthquake that affected the northwestern part of Turkey on August 17, 1999, and in particular the gulf of İzmit, had dramatic consequences also as regards tsunami generation. The main cause of the earthquake was a dextral strike-slip rupture that took place along different segments of the western part of the North Anatolian Fault (WNAF). The rupture process involved not only a number of distinct strike-slip fault segments, but also dip-slip ancillary faults, connecting the main transcurrent segments. The general picture was further complicated by the occurrence of subsidence and liquefaction phenomena, especially along the coasts of the İzmit bay and in the Sapanca Lake. Tsunami effects were observed and measured during post-event surveys in several places along both the northern and the southern coasts of the bay. The run-up heights in most places were reported to lie in the interval 1–3 m: but in the small town of Değirmendere, where a local slump occurred carrying underwater buildings and gardens of the waterfront sector, eyewitnesses reported water waves higher than 15 m.

The purpose of this work is to investigate on the causes of the tsunami by means of numerical simulations of the water waves. We show that the tsunami was a complex event consisting at least of the combination of a regional event due to tectonic causes and of a local event associated with the mass failure. As to the first, we are able to demonstrate that the observed tsunami cannot be explained only in terms of the sea bottom dislocation produced by the main right-lateral dislocation, but that the prominent contribution comes from the displacement associated with the secondary shallow normal faults. Furthermore, the large waves and effects seen in Değirmendere can be explained as the consequence of the slump. By means of a stability analysis based on an original method making use of the limit equilibrium concept, we show that the slump was highly stable before the earthquake and that it was triggered by seismic waves. Simulation of the tsunami induced by the slump was carried out by a two-step numerical code that computes the landslide motion first, and then the generated water wave propagation. It is shown that the computed local tsunami matches the experimental data.


*Keywords:* 1999 Kocaeli earthquake; tsunami modeling; earthquake-induced tsunami; slump-induced tsunami

* Corresponding author. Tel.: +39 051 2095025; fax: +39 051 2095058.
*E-mail address:* steve@ibogfs.df.unibo.it (S. Tinti).

0025-3227/$ - see front matter © 2005 Elsevier B.V. All rights reserved.
doi:10.1016/j.margeo.2005.09.010

## 1. Introduction

### 1.1. Tectonic setting and earthquakes

The Anatolian peninsula is one of the most seismically active areas in the world. The 1999 Kocaeli earthquake and the associated İzmit bay tsunami are the last catastrophic occurrences of a long series of disastrous and lethal natural events that hit this region. Here earthquake generation is governed chiefly by three main tectonic structures: the East Anatolian Fault (EAF), the North Anatolian Fault (NAF) and the Hellenic Arc (Fig. 1). The left-lateral EAF is circa 550 km long and represents the border between the Anatolian

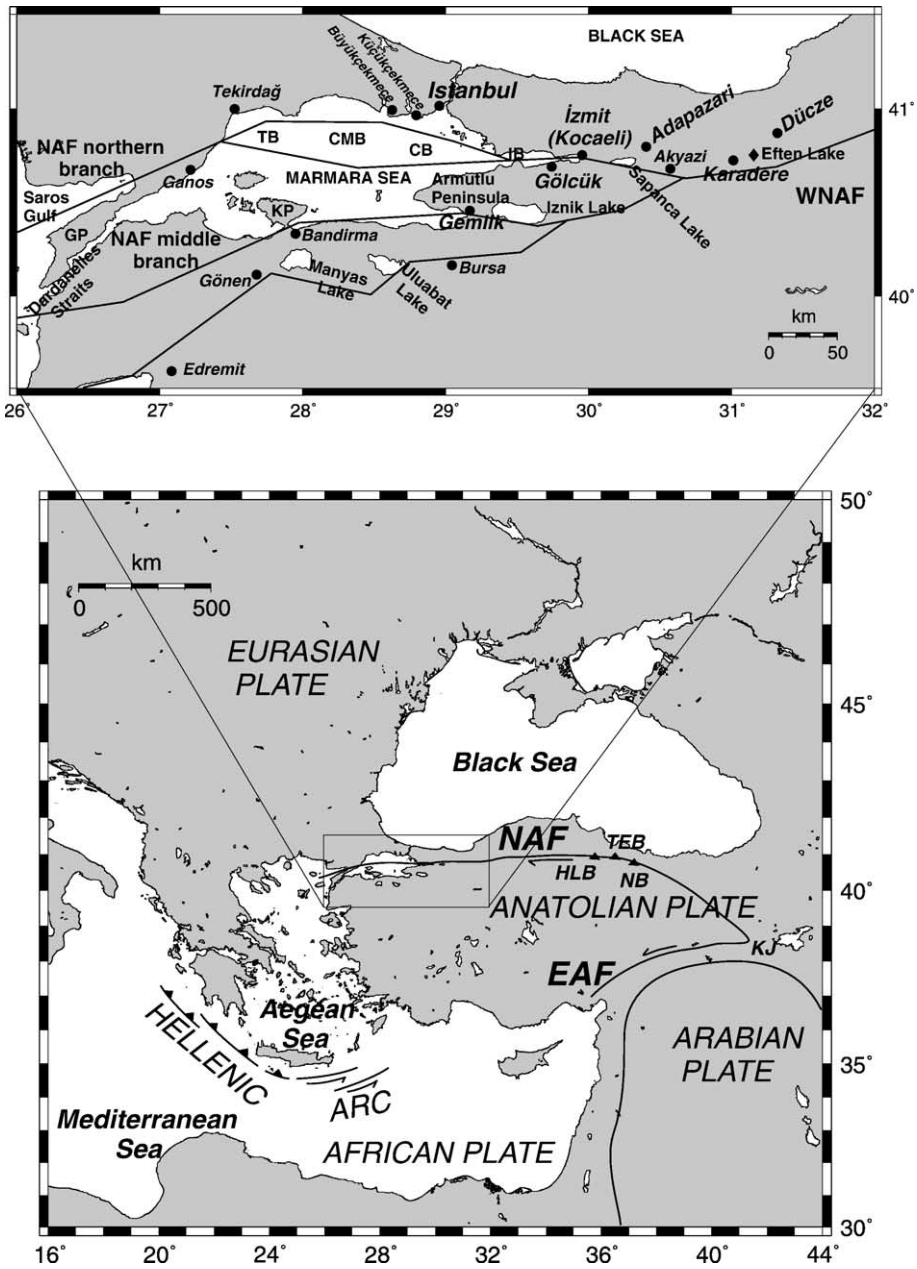


Fig. 1. Upper panel: Sketch of the Marmara Sea crossed by the Western section of the North Anatolian Fault (WNAF) system, which splits into three branches: northern, middle and southern branch. TB, Tekirdağ Basin; CMB, Central Marmara Basin; CB, Çinarcik Basin; IB, İzmit Bay; KP, Kapidağ Peninsula; GP, Gelibolu Peninsula. Lower Panel: The WNAF is part of the complex fault pattern resulting from the Anatolian Plate dynamics. KJ, Karlıova Junction; NB, Niksar Basin; TEB, Taşova-Erbaa Basin; HLB, Havza-Ladik Basin.

block and the Arabian plate. The NAF is a dextral system of faults forming the broad arc boundary between the Eurasian plate and the Anatolian block. It extends for about 1500 km from the northern Aegean Sea, through the Marmara Sea up to the easternmost part of Turkey where it connects to the EAF at the Karliova triple junction. Its western section, denoted hereafter as WNAF, splays into two branches (Fig. 1), approximately in correspondence of the Mudurnu Valley fault, east to Akyazi (Barka and Kadinsky-Cade, 1988; Barka, 1992; Gülen et al., 2002). The northern one starts from the North Aegean Sea, trending NE along the gulf of Saros; then it crosses west–east the central and northern section of the Marmara Sea where it broadens in a wide complex of strike-slip and dip-slip faults; next, it penetrates in the İzmit bay, whence it continues towards the Sapanca Lake, further joining the main NAF system (Barka and Kadinsky-Cade, 1988). A number of large historical earthquakes are associated with this branch. For example, fault rupture migrated from east to west in the 18th century involving progressively all this system of faults from İzmit to Şarköy, first with the 1719 (İzmit, $M_S$ 7.4), and then with the 1754 (eastern Marmara, $M_S$ 6.8) and with the May (eastern Marmara, $M_S$ 7.1) and August (Ganos, $M_S$ 7.4) 1766 shocks (Ambraseys and Finkel, 1995; Ambraseys, 2002a). Notice that westward migration of seismicity has been identified in several sequences of earthquakes also along the main section of the NAF and may be related to the basic long-term tectonic processes of inter-plate interaction going on here (Barka, 1992; Armijo et al., 1999; Hubert-Ferrari et al., 2002). Later, major quakes that are attributed to segments of this branch occurred in 1878, in 1894 ($M_S$ 7.3) and in 1912 ($M_S$ 7.4) (Ambraseys and Finkel, 1991; Ambraseys, 2002a). The most recent occurrences are the 1943 ($M_S$ 6.4) Hedek-Adapazari earthquake and the 1963 ($M_S$ 6.4) Çinarcik earthquake. This is also the genetic place of the Kocaeli earthquake that is at the centre of our attention here, being the cause of the 1999 İzmit tsunami.

The southern branch splits in turn into two further strands east to the Iznik Lake (Fig. 1), which makes that the total number of the WNAF branches can be considered to be three: these further subsystems can be called the middle and the southern branch of the WNAF. The middle runs NE-ward from the Aegean Sea, south of the Dardanelles Straits, and intersects the southern coast of the Marmara Sea around Bandırma. From here it parallels the coastline up to the Gemlik bay, south of the Armutlu peninsula. The WNAF southern branch trends almost parallel to the middle, some tens of kilometers to the south, passing through the Manyas and the Uluabat lakes and through the area of Bursa (Gülen et al., 2002). Historical earthquake activity seems to be more intense on the southern than on the middle branch of the WNAF. Several large earthquakes are known to have occurred here in the last three centuries. The most recent sequence of major quakes manifested as an eastward migration of rupture starting with the October 6, 1944 ($M_S$ 6.8) Edremit-Ayvalik earthquake, with epicentre of 26.56°E, 39.48°N (earthquake database of Bosphorus University, Kandilli Observatory, and Earthquake Research Institute (KOERI), available at http://www.koeri.boun.edu.tr/jeofizik/defaulteng.htm), and continuing with the March 18, 1953 ($M_S$ 7.2) Yenice-Gönen quake with epicentre of 27.36°E, 39.99°N (KOERI database), probably occurring on the middle branch, and with the October, 06, 1964 ($M_S$ 6.9) Manyas-region shock: epicentre 26.23°E, 40.30°N (KOERI database). Hence the sequence affected the overall sector from the Aegean Sea up to the Uluabat Lake (Hubert-Ferrari et al., 2000; Ambraseys, 2002a; Barka et al., 2002).

### 1.2. Transtensional tectonics and pull-apart basins

Due to the collision between the Arabian and Eurasian plates, the Anatolian plate is squeezed and pushed westward moving along the NAF and EAF. The tectonic style is predominantly transcurrent along the NAF system, where slip occurs along a series of faults tens of kilometers long with prevailing EW trend. But at the junction of several of such segments, due to their relative offset and overstepping, extensional tectonics occurs with the consequent formation of a sequence of pull-apart basins, such as the prominent depressions of the Niksar, of the Taşova-Erbaa and of the Havza-Ladik basins that one finds in the central portion of the NAF (Barka et al., 2000). In the WNAF, step-over depressions on land are often associated with lakes (e.g. the Sapanca Lake in the northern branch of the WNAF, the Iznik Lake in the middle strand and the Uluabat and the Manyas lakes in the southern branch). Transtension and vertical movements are believed to be of foremost importance especially on the northern branch of the WNAF. Indeed the genesis of the Marmara Sea itself is attributed to pull-apart processes (Hubert-Ferrari et al., 2002). More specifically, overstepping may be advocated to explain the formation of the three main inner basins characterising the Marmara Sea (see Armijo et al., 2002; Flerit et al., 2003) that from west to east are the Tekirdağ basin, the Central basin and the Çinarcik

basin, separated from one another by bathymetric highs (Fig. 1; see Le Pichon et al., 2001). And analogously, processes associated with fault segment step-overs may be invoked also to interpret the morphological structure of the 50 km long and 10 km wide İzmit bay, where three distinct sub-basins can be identified (Fig. 2): the western basin, which is the deepest one, and opens into the Marmara Sea, the Karamürsel basin (central basin) with maximum depth around 200 m, and the eastern basin, hereafter named the İzmit basin that is very shallow being at most 40 m deep (Lettis et al., 2002; Kuşçu et al., 2002).

### 1.3. Tsunamis

A long history of tsunami occurrences is associated with the earthquakes in the coastal and submarine segments of the WNAF, and especially of the northern strand. As many as circa 100 tsunami events are reported in tsunami catalogues of Turkey, starting

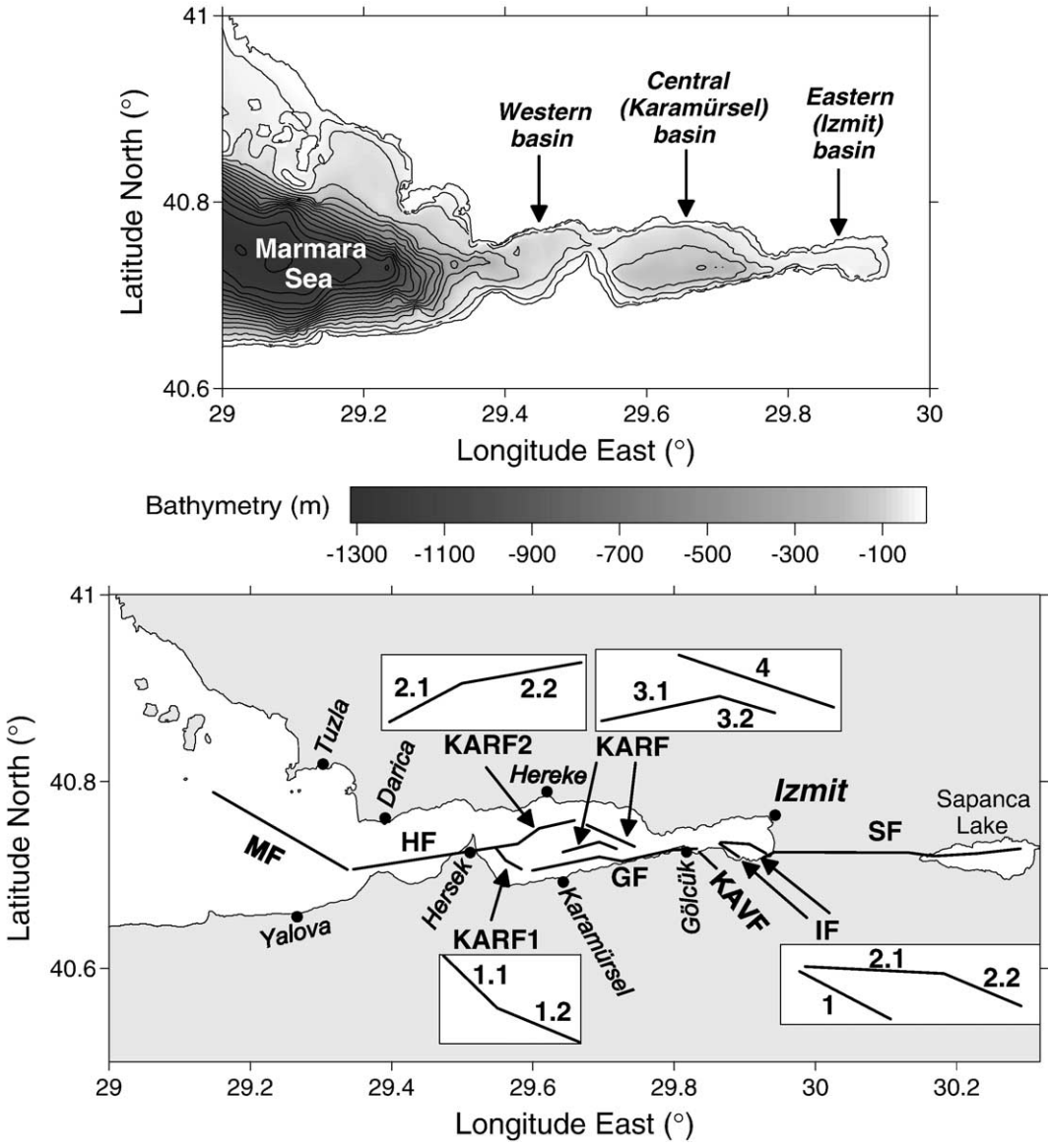


Fig. 2. Fault system in the eastern part of the Marmara Sea that is assumed to be involved in the tsunami generation (lower panel). It is composed by strike-slip faults (i.e. the Marmara, MF, the Hersek, HF, the Gölcük, GF, and the Sapanca fault, SF), and by normal faults (i.e. the Karamürsel faults, KARF1, KARF2, KARF3 and KARF4, the Kavakli fault (KAVF) and the İzmit faults (IF1 and IF2)). Fault parameters are listed in Table 2. Names and bathymetry of the basins forming the İzmit bay are given in the upper map.

from the Minoan Santorini explosion tsunami in the Aegean Sea until the recent 1999 Kocaeli-earthquake tsunami that is treated here (see Altinok and Ersoy, 2000; Papadopoulos, 2001; see also Ambraseys, 1962; Kuran and Yalçiner, 1993). Practically, according to historical records, all the Turkish coasts were affected: the Black Sea coastline to the north (Yalçiner et al., 2004), the Aegean coast to the west and the eastern Mediterranean coasts (Yalçiner et al., 2001a,b), but one of the largest concentration of cases is found in the Marmara Sea and in the İzmit bay. Historical information on tsunamis in Turkey, as in all the other European countries and in many other countries in the world, is generally insufficient for a statistical analysis of the tsunami hazard and for a proper characterisation of the tsunami effects. Reports are mostly sporadic and detailed descriptions are available only for a restricted number of cases. Moreover, the reliability of the historical sources is not always sound. In a recent study on the Marmara Sea tsunamis, Ambraseys (2002b) concluded that about 50% of the cases found in the literature are to be ruled out as spurious events. Nonetheless, this region remains one of the European areas with the highest tsunami activity, and most vulnerable to tsunami attacks. Interest for the evaluation of the tsunami risk in the whole region of the Marmara Sea has increased after the occurrence of the 1999 Kocaeli earthquake and tsunami, and after the speculation based on stress-transfer theory that its occurrence has highly favoured the condition for the next WNAF rupture to take place in the submarine section of the northern strand (Hubert-Ferrari et al., 2000; Parsons et al., 2000; Parsons, 2004). A possible future earthquake occurring in the Marmara Sea has a direct tsunamigenic potential, and, furthermore, may set in motion submarine masses (landslides or slumps), with additional possibility to produce tsunamis. Signatures of past mass failures have been identified in several places by specific and very detailed marine geological surveys in several places of the sea of Marmara (see e.g. Altinok et al., 1999; Alpar and Yaltirak, 2002; Yüksel et al., 2002), and scenarios of tsunamis induced by earthquake-triggered underwater slides have been analysed by Yalçiner et al. (2002), with the conclusion that risk associated with tsunami occurrence is a very serious issue especially in the İstanbul area.

## 2. The Kocaeli earthquake and its genetic fault system

The Kocaeli earthquake struck in the night of August 17, 1999 at 3:02 AM and affected a very vast region from the Eften Lake, east of Karadere, to the whole İzmit bay. The areas with the largest toll of destruction and damage were the district of Adapazari and the belt around the eastern and southeastern coast of the İzmit bay, but the earthquake was damaging also west of İstanbul where severe effects were observed in the coastal towns of Büyükçekmece and Küçükçekmece in the district of Avcilar. The earthquake was lethal, killing more than 17,000 people. The number of injuries exceeded 43,000, and as many as about 250,000 people remained homeless, implying property losses in the range of $6.5 billion (USGS Report, 2000). The magnitude was estimated to be $M_W$=7.4 by Kandilli Observatory and the epicentre was located at 40.8°N and 30°E (with hypocentre around 17 km depth) near the eastern end of the İzmit bay (Barka et al., 2002). Shaking lasted about 45 s and was recorded by several strong motion sensors placed around and very near to the source (managed by the Earthquake Research Department of General Directory of Disaster Affairs of Turkey). The highest recorded ground acceleration was 0.45 g at the station of Sakarya, to the east of the Sapanca Lake. The earthquake ruptured at least five segments of the northern branch of the NAF, each with length in the range of 20–35 km that from east to west are the Karadere segment, the Sapanca-Akyazi segment (to the east of the Sapanca Lake), the Sapanca segment (to the west of the lake), the Gölcük segment and the Hersek segment (Barka et al., 2002; Lettis et al., 2002). The tsunamigenic fault segments are sketched in Fig. 2. Aftershock distribution and SAR data analysis possibly suggest that rupture took place also on a further segment in the Marmara Sea to the east of the İzmit bay entrance (Gülen et al., 2002; Çakir et al., 2003). The areas connecting the fault segments have been recognised as distinct right-releasing step-over regions, whose width goes from 1 to 2 km for the Sapanca Lake and the Gölcük step-overs up to 4–5 km for the Karamürsel step-over (Lettis et al., 2002). Slip distribution deduced from seismological records and from field surveys of the surface breaks shows that slip was highly heterogeneous along the fault and that the maximum values of dextral displacement have to be assigned to the Sapanca-Akyazi segment (5–6 m) and to the Gölcük segment (4–5 m) (Barka et al., 2002; Lettis et al., 2002), a picture that is basically further confirmed by inversion of GPS and satellite data (Feigl et al., 2002; see also Delouis et al., 2002, whose study identifies a third area of increased slip in the westernmost sector of the İzmit bay) as well as by combining tectonic observations and SAR data (Çakir et al., 2003).

The multiple-rupture main shock was dominated by the right-lateral strike-slip component in agreement with the dominant tectonic style of the region. Consistently, observed ground movement was typically horizontal. However, also vertical ground movements were identified in several places in a narrow belt along the main fault-segments zone. Coastal subsidence was observed in the southern coast of the Sapanca Lake and in the southeastern coast of the İzmit bay, and caused extensive flooding and permanent retreat of the shoreline by tens to hundreds of meters. The observed vertical displacements can be accounted for only partially by the strike-slip source model, and require a different explanation, namely liquefaction and normal faulting. Ground sinking due to widespread liquefaction phenomena was ascertained to have occurred in Adapazari where several hundreds of buildings were affected (USGS Report, 2000). Liquefaction was also observed in Sapanca as well as in the delta fan east of Gölcük (Sucuoğlu et al., 2000).

Ancillary normal faults with dominant vertical component in addition to a smaller right-lateral slip were mapped in several places. The most relevant one was seen east of Gölcük in the locality known as Kavakli, and was the main cause of the subsidence that affected Gölcük (Rothaus et al., 2004). The fault, trending NW–SE, can be traced for a 3.5 km inland, intersects the coastline, and probably continues offshore. The scarp shows a vertical offset of about 2 m and a typical dextral offset of 0.40–0.60 m that were measured by several surveying teams (Barka et al., 2002; Lettis et al., 2002), one of which was a joint Italian-Turkish (IT) team and included four of the authors of the present paper (namely Tinti, Armigliato, Yalçiner and Altinok). The role of surface normal faulting was probably minor in determining the major catastrophic ground shaking that is to be attributed more appropriately to the ruptures along the long dextral fault segments. But the point of this paper is that these faults were essential in the genesis of the tsunami. Seismic profiles taken after the occurrence of the Kocaeli earthquake show the clear signature of the main fault zone that disturbed the underwater sediments (Alpar, 1999). However, beyond the main fault system, offshore normal faults were identified by means of bathymetric and shallow seismic data in the central (Karamürsel) and in the eastern parts of the İzmit bay (Şengör et al., 1999; Alpar and Yaltirak, 2002; Lettis et al., 2001, 2002), and their trend and position is consistent with the vertical dynamics that is associated with the formation of these step-over basins.

## 3. Tsunami observations

The 1999 Kocaeli earthquake caused a tsunami that was observed in the entire İzmit bay. Unfortunately no tide-gauge records are available for the tsunami either in the source region or in the Marmara Sea. Post-event field surveys and interview of eyewitnesses conducted soon after the tsunami occurrence by several teams enabled to determine the coastal areas of major wave impact and to quantify the run-up heights and the sea penetration lengths in all the affected places. The tsunami was observed soon after the main shock. Almost in all places the tsunami was seen to cause the sea to withdraw first and then to overcome the usual shoreline and inundate land. The observed tsunami run-up heights were modest and typically in the range of 1–3 m. The tsunami was damaging, but not catastrophic. In some places it was strong enough to carry boats and vessels on land. One example comes from Yeniköy, east of Kavakli, where a large floating platform, 60 m long and 12 m wide that was used as a pier, was moved and transported about 100 m on land over a grassy stretch of coast (Altinok et al., 2001; Rothaus et al., 2004). A detailed description of the tsunami observations can be found in the works by Yalçiner et al. (2000, 2001a,b,c) and by Altinok et al. (2001), and has been integrated in a recent study by Rothaus et al. (2004) that focuses on the effects in the southern coast of the İzmit bay. Table 1 summarises the observations on first arrival, water penetration and run-up heights that can be found in the aforementioned papers, and complements the data set by adding new observations, so far unpublished that were collected during the IT post-event field survey.

The tsunami was exceptionally violent only in the town of Değirmendere. Here measured wave run-ups exceeded 4 m, but several eyewitnesses state that the wave reached the second floor of the buildings in the waterfront (IT), and some other estimate a height of about 15 m (Rothaus et al., 2004). Ships moored in the port of Değirmendere were severely affected by the waves and seamen told that the attacking wave was probably larger than 10 m (Altinok et al., 2001). Perhaps the same large wave struck ships moored in the next town of Kavakli, east of Gölcük: here the tsunami came over a ship reaching a height of more than 15 m, according to witnesses rough evaluation (Rothaus et al., 2004). The anomalous violence of the tsunami in the limited area around Değirmendere is the consequence of an additional local tsunamigenic source that was identified in a slump. A stretch of coast about 300 m long (parallel to shoreline) and 75 m wide (perpendicular to shoreline), where a recreational area called

Table 1
Post-tsunami field survey observations

| Locality | Locality code[a] | Survey | First arrival | Penetration length (m) | Observed run-up height (m) |
|---|---|---|---|---|---|
| Darıca | 1 | AL | | 4 | >1 |
| Eskihisar | 2 | AL | | 15 | >1 |
| Dilovasi | 3 | AL | – | | 2 |
| Tavşancıl | 4 | AL | – | 25–30 | 1.5 |
| | | IT | – | 25 | 1.7–2.5 |
| Hereke | 5 | AL | | 30 | 1.8 |
| | | IT | | | 2.25–2.9 |
| Şirinyali | 6 | AL | | 15 | >2 |
| Kirazliyali | 7 | AL | | | 2.5 |
| Yarımca | 8 | AL | – | >60 | |
| | | IT | – | | 3.2 |
| Körfez | | AL | | 100 | |
| Tupras (Kiler Point) | 9 | AL | | 20 | 2.5 |
| Derince Port | 10 | AL | – | | 2–2.5 |
| Çene Suyu | 11 | AL | – | 60 | 2? |
| İzmit, Marina | 12 | AL | – | 25 | |
| Seymen (Yeniköy) | 13 | AL | | 50 | |
| | | IT | | 50 | 2 |
| | | RO | | >200 | |
| Kavakli | 14 | AL | | 300? | |
| Gölcük | 15 | RO | | | 15–20[b] |
| Değirmendere | 16 | AL | – | 35? | 2.5 |
| | | IT | – | | 2.4 |
| | | RO | – | 80 | 4.4 (15[b]) |
| Halidere | 17 | AL | – | 60 | 0.8 |
| | | IT | – | 47–92 | 1.5 |
| Ulasli | 18 | AL | – | >5 | 2 |
| Eregli-Guzelyali | 19 | AL | + | 4 | 1.25 |
| Defne Mahallesi | 20 | AL | | 4 | 1.5 |
| Karamürsel | 21 | AL | – | | |
| Kaytazdere | 22 | AL | | 15? | |
| Hersek | 23 | AL | | >30 | |
| | | RO | | 15 | |
| Havuzdere | | AL | | | |
| Topçular | 24 | AL | – | | 2? |
| Offshore Topçular | | AL | | 30? | 30? |

AL: survey by Altinok et al. (2001); IT: survey by Italian-Turkish team composed by Altinok Y., Armigliato A., Bortolucci E., Guidi C., Tinti S., Yalçiner A.C.; RO: survey by Rothaus et al. (2004).
[a] Localities are numbered as in Fig. 3.
[b] Not run-up height value, but wave height offshore reported by eyewitnesses.

Çinarlik Park was located, slid into the sea, carrying a multi-storing hotel, owned by the municipality, a cafe and a restaurant and 14 park trees (Arel and Kiper, 2000; Altinok et al., 2001; Cetin et al., 2004). Modeling of both the tectonic tsunami and the local tsunami induced by the coastal mass failure is the main aim of this work and will be tackled with the appropriate attention in the following.

## 4. Simulations of the earthquake-induced tsunami

Tsunami simulations are based on a finite-element model solving the non-linear shallow water equations that has been developed specifically for tsunami analysis by the University of Bologna, Italy, and has been extensively used to study near-field propagation of tsunamis generated by near-shore earthquakes (Tinti et al., 1994; among the applications, see Piatanesi and Tinti, 1998, 2002; Tinti and Armigliato, 2003). The İzmit bay and the easternmost part of the Marmara Sea facing the bay have been covered by a grid consisting of 11,006 nodes and 20,197 triangles, having a space resolution variable from place to place (coarser in deep water and finer in shallow coastal areas). The grid that is portrayed in Fig. 3 was created through a mesh building code optimised for tsunami simulations that is suited to basins with complex bathymetries and irregular coastlines and that tends to produce triangles with the highest index of isotropy (typically equilateral) and a uniform crossing time (Tinti and Bortolucci, 1999). The coastal boundary is delimited by vertical walls causing total reflection of the water waves. Technically, this means that the tsunami model does not compute the tsunami run-up heights, but only the maximum water elevation (MWE) at the vertical coast. However, this is not a significant limitation for the purpose of this paper, since MWEs are known to be a reasonable approximation of run-up heights for most coastal morphologies. The depth data set has been assembled by digitising nautical maps of the Marmara Sea (1:300,000) and of the İzmit bay (1:50,000) published by the Hydrographic and Oceanographic Service of Turkey and by digitising maps from Lettis et al. (2002) that are based on recent data gathered by the Turkish Navy and by Güneysu (1999). This bathymetry data set has been further integrated with depth data collected in the course of the post-tsunami survey by the IT team. Fig. 2 provides a map with the bathymetry and Fig. 3 shows the grid and localities where tsunami observations were made and/or tsunami time histories and maximum water elevations have been calculated.

The faults used to generate the numerical tsunami are listed in Table 2. As regards the main strike-slip faults, we consider only those fault segments that are found close enough to the water basin to cause deformation of the sea bottom. Therefore neither the Karadere segment nor the Sapanca-Akyazi segment are

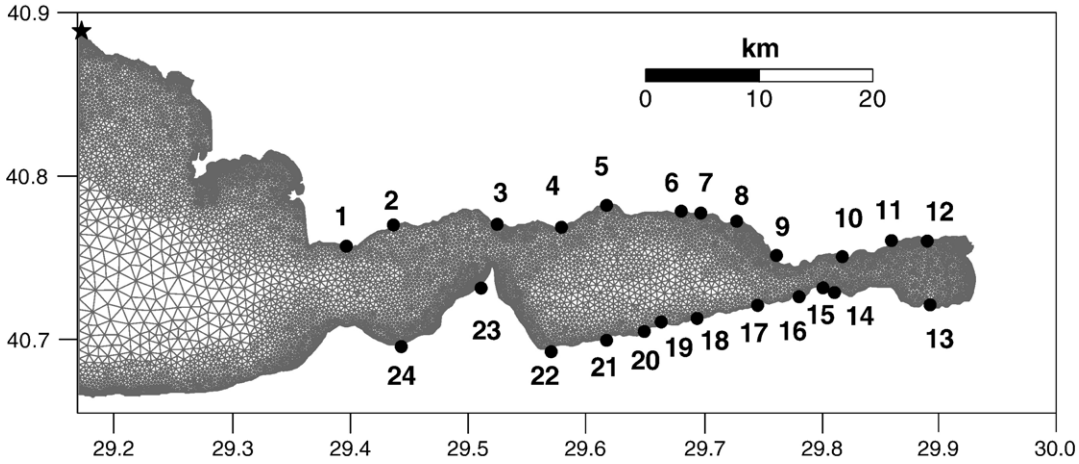


Fig. 3. Grid used for the numerical simulation of the earthquake-induced tsunami, consisting of 11,006 nodes and of 20,197 triangles. Numbers refer to places where tsunami observations of the post-event surveys were made (see Table 1): (1) Darica, (2) Eskihisar, (3) Dilovasi, (4) Tavşancil, (5) Hereke, (6) Sirinyali, (7) Kirazliyali, (8) Yarimca, (9) Tupras, (10) Derince, (11) Cene Suyu, (12) İzmit, (13) Seymen, (14) Kavakli, (15) Gölcük, (16) Değirmendere, (17) Halidere, (18) Ulaşli, (19) Eregli, (20) Defne, (21) Karamürsel, (22) Kaytazdere, (23) Hersek, (24) Topçular.

taken into account. The faults supposed to contribute to the tsunami are from east to west the Sapanca fault (SF), the Gölcük fault (GF) and the Hersek fault (HF). We also add the Marmara fault (MF) that is totally submarine and that, according to some studies (Gülen et al., 2002; Çakir et al., 2003), represents the westernmost rupturing segment of the Kocaeli earthquake, although this point of view is not unanimously agreed upon. Fault parameters are derived from the literature, which is properly acknowledged in the caption of Table 2. Some of these faults are subdivided in a number of rectangular uniform-slip sub-faults to approximate bet-

Table 2
Parameters for the tsunamigenic strike-slip (grey background cells) and normal faults

| Fault | Fault code | Slip (m) | Width (km) | Length (km) | Strike (degree) | Dip (degree) | Rake (degree) |
|---|---|---|---|---|---|---|---|
| Marmara Fault (Gülen et al., 2002) | MF | 1.0 | 17.5 | 18.4 | 120 | 90 | 180 |
| Hersek Fault (Lettis et al., 2002) | HF | 1.3 | 20 | 19.8 | 81 | 90 | 180 |
| Gölcük Fault (Barka et al., 2002) | GF1 | 4.1 | 10 | 8.1 | 79 | 90 | 180 |
| | GF2 | 4.1 | 10 | 2.8 | 101 | 90 | 180 |
| | GF3 | 4.1 | 10 | 6.0 | 77 | 90 | 180 |
| | GF4 | 4.1 | 10 | 3.0 | 87 | 90 | 180 |
| Sapanca Fault (Lettis et al., 2002) | SF1 | 5.3 | 10 | 1.5 | 64 | 90 | 180 |
| | SF2 | 5.3 | 10 | 16.1 | 90 | 90 | 180 |
| | SF3 | 5.3 | 10 | 3.0 | 97 | 90 | 180 |
| | SF4 | 5.3 | 10 | 5.2 | 87 | 90 | 180 |
| | SF5 | 5.3 | 10 | 5.1 | 84 | 90 | 180 |
| Karamürsel Fault (Lettis et al., 2002) | KARF1.1 | 2.0 | 3 | 2.0 | 142 | 120 | 90 |
| | KARF1.2 | 2.0 | 3 | 2.1 | 119 | 120 | 90 |
| | KARF2.1 | 2.0 | 3 | 3.2 | 54.2 | 60 | 270 |
| | KARF2.2 | 2.0 | 3 | 4.3 | 77.3 | 60 | 270 |
| | KARF3.1 | 2.0 | 3 | 4.5 | 74 | 60 | 270 |
| | KARF3.2 | 2.0 | 3 | 2.2 | 112 | 60 | 270 |
| | KARF4 | 2.0 | 3 | 6.2 | 114 | 60 | 270 |
| Kavakli Fault (Lettis et al., 2002) | KAVF | 2.0 | 3 | 2.8 | 134 | 120 | 90 |
| | | 0.6 | | | | 120 | 180 |
| İzmit Fault (Barka et al., 2002) | IF1 | 2.0 | 3 | 2.7 | 125 | 120 | 90 |
| | IF2.1 | 2.0 | 3 | 3.4 | 94 | 60 | 270 |
| | IF2.2 | 2.0 | 3 | 2.2 | 119 | 60 | 270 |

Slip amount, length and width of all strike-slip faults are taken from Gülen et al. (2002).

ter the along-fault variable strike. The slip varies in a range of 1.0 m to 5.30 m, increasing from west to east.

The dip-slip faults taken into account in our study are the Kavakli fault (KAVF) and all the faults corresponding to the step-over regions of the Karamürsel (KARF) and of the İzmit (IF) sub-basins (see Table 2). The only inland fault is the Kavakli fault: for this fault, strike, length and slip values come from measurements taken in the field (Barka et al., 2002; Lettis et al., 2002, and IT team observations), and there is clear evidence that it ruptured during the Kocaeli earthquake. The submarine normal faults are determined on the basis of bathymetric and shallow seismic surveys (Şengör et al., 1999; Lettis et al., 2001, 2002), but there is no certainty that they were active during the main quake. Here we assume that all these faults have dip of 60° and are very shallow (fault width is supposed to be 3 km), being surface expression of the stress accommodation processes associated with the step-overs. We assume further that they were involved in the main shock process with a slip amount comparable with the Kavakli fault (see Table 2).

The initial tsunami energy is assumed to be only potential with water elevation field taken to be equal to the coseismic vertical displacement field of the seafloor, which is usual in simulations of tsunamis induced by earthquakes. Surface coseismic deformations are calculated through Okada's (1992) formulas, holding for rectangular faults buried in a homogeneous elastic half-space. Since Okada's model is based on elastic linear theory, the displacements produced by multiple rectangular sources can be superposed in order to obtain the total coseismic ground displacement and, consequently, the initial seawater elevation condition.

Our study intends to demonstrate that the tsunami data cannot be explained only by the strike-slip fault sources that were responsible for the catastrophic main ground shaking, and that additional sources are needed in order to justify the observations. We suggest that these additional sources may be found in the set of coastal and submarine normal faults listed in Table 2. To this purpose we analyse the tsunamigenic effects of the strike-slip fault system first, and then we add the further contribution of the normal faults. As to the right-lateral fault tsunami, we run two different experiments, one with the sources involving the İzmit bay, namely the three fault segments HF, GF and SF, and the other with the supplementary addition of the Marmara fault (MF), whose role is not unanimously recognised. Fig. 4A exhibits the curves of the MWE computed along the coastal nodes of the basin for the strike-slip tsunami sources. The starting point is the coastal node in the upper left corner of the mesh (Fig. 3), corresponding to the westernmost position on the northern coast. The coastline is run clockwise, reaching the lower left corner. Relevant localities are all within the İzmit bay and are identified with numbers in the grid map given in Fig. 3 that are repeated in Fig. 4 to help the reader. The results of the two simulations, with and without MF, are very similar, with a slight difference that can be noted only for the coastal nodes that are found outside the İzmit bay (plotted at the initial and ending part of the graph), which means that the tsunamigenic effect of MF is not relevant. Therefore, it will not be considered any longer in our analysis. The most important outcome of the tsunami simulation is that the calculated MWE are very low along the entire coast of the bay with values that are typically less than 30 cm and occasional peaks around 50–70 cm. This is at odd with the run-up height observations and is a very strong element proving our thesis that the dextral fault system of the Kocaeli earthquake is not able to generate a significant tsunami.

In the second stage of the analysis we invoke the contribution of the normal faults given in Table 2. The MWE corresponding to the case of the sole normal-fault system and to the case of the ensemble of all the active faults (strike-slip and normal) with the exception of MF are plotted in Fig. 4B. Furthermore, also the observed run-up heights are added to the graph. The two curves are found to differ insignificantly from one another, which shows that the contribution of the normal-fault sources is highly predominant in determining the resulting MWE values. Most importantly, the comparison between the calculated curves and the measured run-up heights shows that the agreement is acceptable, though not yet perfect. Though there are some zones of marked overestimation (e.g. the peak around point 20 corresponding to Defne Mahallesi), a general underestimation of the experimental data can be noted, which is however mild and can be probably reduced or even eliminated by tuning the sources. The only town where the computed wave elevations are largely inconsistent with observations is Değirmendere, where the tsunami has to be explained as the effect of the coastal slump, as will be shown in detail in the next section. Fig. 5 depicts some of the tide-gauge records computed both on the northern and on the southern coast of the bay for the case of the combined normal and strike-slip faults. The curves are identified by numbers that correspond to the locality numbers shown in the map of Fig. 3 and also given in Table 1. Records either show a negative first

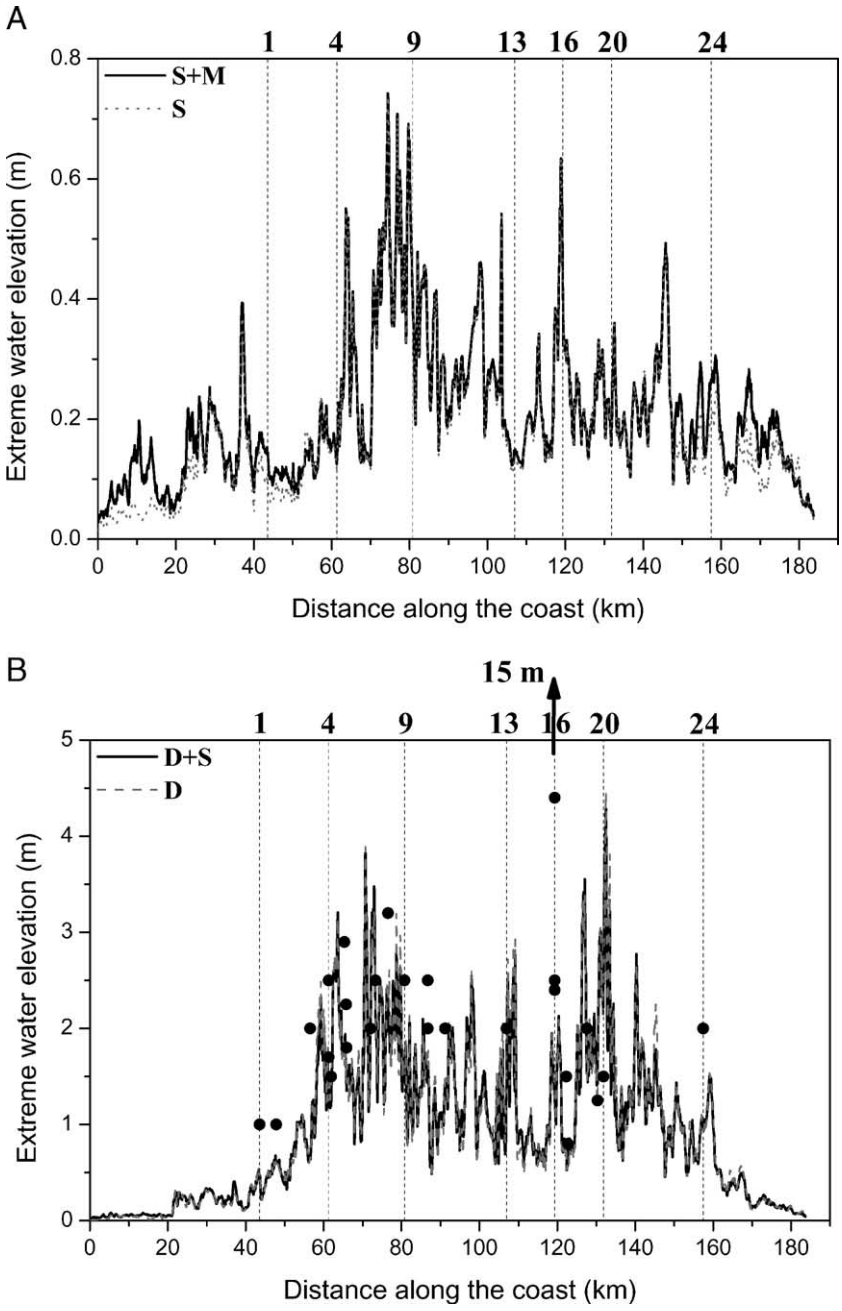


Fig. 4. Maximum water elevation computed for the coastal nodes calculated for the tsunamis induced by different set of sources. (A) All strike-slip sources either including the Marmara Fault (S+M) or excluding it (S). (B) All dip-slip faults (D) and dip-slip together with strike-slip faults (D+S). Faults are listed in Table 2 and graphed in Fig. 2. Distances on the horizontal axis are measured along the coast from the upper left corner of the grid given in Fig. 3 and numbers correspond to the localities on the same figure. Solid circles in panel (B) are the observed run-up heights given in Table 1. Maximum values reported in Değirmendere (15 m) go out of scale.

arrival or a very small positive arrival that is followed by a much larger sea level lowering, which is in agreement with most accounts of eyewitnesses who observed a sea retreat first (the idea is that the initial sea rise was so small that passed unobserved to people). In most places the largest oscillations occur in the first 5–10 min after the shock with dominant period of 3–4 min, and are later followed by a long train of small slow-decay oscillations also with longer period. The complex structure of the marigrams

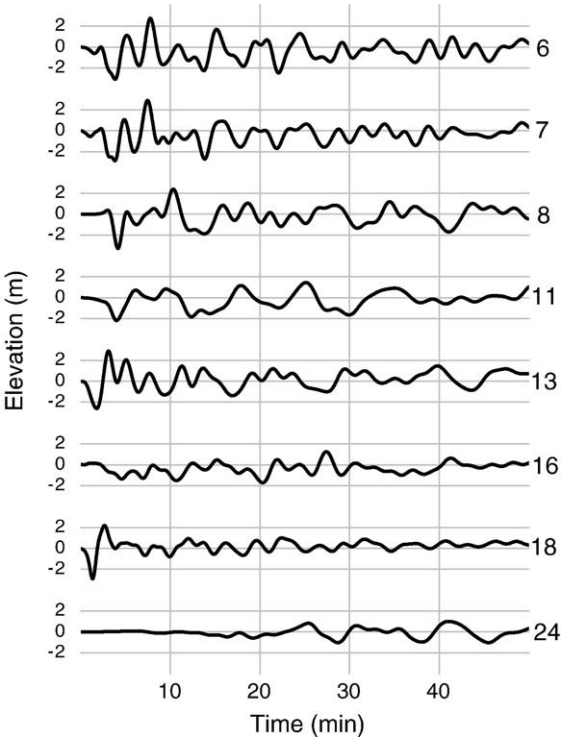


Fig. 5. Computed tide-gauge records for the tsunami induced by all faults, but the Marmara fault (case D+S of Fig. 4) for the localities identified by the numbers on the right.

reflects the complexity of the sources and of the basin morphology, which favours the onset and persistence of transverse mode of oscillations, corresponding to waves crossing the bay in north–south direction. Record 24 corresponds to Topçular that is found in the outer İzmit bay basin and is far from the normal-fault sources considered here. The tsunami is here quite weak, which shows that the energy tends to remain trapped within the inner basins of the bay with modest outward radiation. Marigram 16 is computed at Değirmendere. The main comment is that the calculated oscillations here are small amplitude, and generally negative in the first post-earthquake 10-min window, during half of which the sea remains below the normal level by about 1–1.5 m. This is a detail that may have some relevance for the stability of the local coastal slope, as will be discussed in the next section.

## 5. The slump at Değirmendere

Değirmendere is a village located in the southern coast of the Karamürsel pull-apart basin (point 16 in Fig. 3). A segment of coast about 300 m long and 75 m wide slid into the sea carrying a multi-storey hotel and two adjacent buildings, and produced a completely new shoreline (Rathje et al., 2002, 2004; Cetin et al., 2004). A more violent tsunami was testified by witnesses and observed by post-event surveys in this area. It started at the same time of the main shock, or with some minutes delay according to only a single account, and manifested first with a seawater withdrawal (Altinok et al., 2001; Rothaus et al., 2004; IT team). In this work, based on data taken from the literature and on data collected by the IT team, first we analyse the stability of the mass involved in the failure, and then we simulate its motion and compute the induced tsunami.

Bathymetric data were collected by a boat survey undertaken around the coast of Değirmendere on October 1999, after the slide, by the IT team. We reconstruct the post-event bathymetry also with the aid of data extrapolated from the article by Cetin et al. (2004). The pre-event bathymetry is derived from the nautical map of the İzmit bay in conjunction with data from Cetin et al. (2004). Pre- and post-failure positions of the coastline are deduced also by making use of the maps by Rathje et al. (2002, 2004). We evaluated the volume of the slump by comparing pre- and post-event bathymetric data in the detachment area, obtaining the figure of $5.18 \times 10^6$ m$^3$.

Post-failure analyses of on-land cracks and geotechnical investigations (borings, as well as in situ SPT, CPT and CPTU tests) carried out in the vicinity of the failed area are available at the web site http://peer.berkeley.edu/turkey/adapazari (Cetin et al., 2004). The analyses show the presence of distinct layers, the surface one (down to a 0.5–1 m depth) consisting of artificial fill of gravely sand and of silty clay. Deeper, one meets a sequence of thicker layers of silty sand, sand and sandy silt with occasional presence of gravel, the underlying bedrock being generally found deeper than 12–15 m (Cetin et al., 2004).

## 6. Stability analysis

The stability study of the Değirmendere slump is carried out here through an original method, hereafter designed as TM method, that is based on the limit equilibrium theory (Tinti and Manucci, in press), but that differs from the classical limit equilibrium methods. Since the method applied is new, we consider it useful for the reader to highlight briefly the main characteristics of this approach. The stability is analysed along 2D cross-sections. As in the classical limit equilibrium methods, the 2D section is partitioned into slices by means of vertical cuts. Imposing the condition of the static equilibrium to all the slices results in a set of three equations (see Fig. 6): two for the horizontal

and vertical forces respectively and one for the torque. In the present formulation they have the following form:

$$\frac{\mathrm{d}}{\mathrm{d}x}E + P\tan\alpha - S - D\tan\beta = -k\cos\psi w$$

$$\frac{\mathrm{d}}{\mathrm{d}x}X + P + S\tan\alpha - D = (1 + k\sin\psi)w$$

$$\frac{\mathrm{d}}{\mathrm{d}x}A - z_1\frac{\mathrm{d}}{\mathrm{d}x}E - D\tan\beta(z_2 - z_1) = -k\cos\psi\, w\frac{z_2 - z_1}{2}$$

Here the coordinate $x$ runs horizontally in the downslope direction. The slide cross-section is bounded by the bottom profile $z_1(x)$ and by the top profile $z_2(x)$, and is assumed to be of unitary transverse width. The local slopes of these profiles are denoted respectively by $\alpha(x)$ and by $\beta(x)$. The quantities appearing in the equations are: the pressure $P$ and the shear stress $S$, acting at the base of the slice respectively in the normal and tangential direction; the hydrostatic load $D$ that is supposedly acting at the top of the slice and is normal to it; the inter-slice force per unit width, decomposed into the horizontal and vertical components $E$ and $X$; the slide weight per unit horizontal length and unit width $w$; and the seismic load, acting at the centre of mass of the slide along the direction determined by the angle $\psi$ (that grows clockwise from the horizontal axis oriented downslope as is shown in Fig. 6) and with magnitude proportional to the slice weight through the coefficient $k$. The variable $A$ in the torque balance equation has the dimension of a torque per unit width and is defined as the first-order moment of the distribution of the horizontal stresses on the vertical downslope face of the slice (see Tinti and Manucci, in press, for all the details). The above set of three equations is complemented by the equation of limit equilibrium based on the Mohr–Coulomb law:

$$FS = c' - u\tan\varphi' + P\tan\varphi'$$

where $c'(x)$ and $\phi'(x)$ are material parameters (cohesion coefficient and friction angle respectively), while $u(x)$ is the pore pressure, depending on the level of the piezometric line. All these functions are allowed to vary downslope, i.e. are supposedly depending on the variable $x$. The quantity $F$ is the factor of safety, which discriminates between a state that for the mass is unstable ($F<1$) and one that is stable ($F>1$).

The boundary conditions to impose at the up-hill and frontal ends of the slide, with respective coordinates $x_\mathrm{i}$ and $x_\mathrm{f}$, concern the components $E$ and $X$ of the inter-slice forces and the torque $A$:

$$E(x_\mathrm{i}) = E(x_\mathrm{f}) = 0$$

$$X(x_\mathrm{i}) = X(x_\mathrm{f}) = 0$$

$$A(x_\mathrm{i}) = A(x_\mathrm{f}) = 0$$

The above system of equations counts as many as five unknown functions, namely $P(x)$, $S(x)$, $E(x)$, $X(x)$ and $A(x)$, and one unknown parameter, i.e. the safety factor $F$. It is underdetermined and admits more than a single solution, since the number of unknowns exceeds the number of constraining equations. Traditional limit equilibrium methods, such as Bishop's, Janbu's, Spencer's, Morgenstern and Price's, etc., seem to overlook the problem, under the assumption that what matters is the value of the factor of safety $F$, and non-uniqueness has only a minor effect on it. In other words, it is traditionally believed that though many (virtually, an infinite number of) solutions can be found, the resulting value of $F$ varies in an acceptably narrow range. We were able to show that this opinion is not well founded, since exact solutions can be found that correspond to a very large range of $F$, both below and beyond the critical value of 1. Consequently, this means that usually there exist solutions showing that the slope is unstable as well as solutions pointing conversely to a slope stability. In order to overcome this basic drawback, we developed a new approach by introducing a new parameter we call the lithostatic deviation $\delta$, which is expressed as the dimensionless ratio of the average

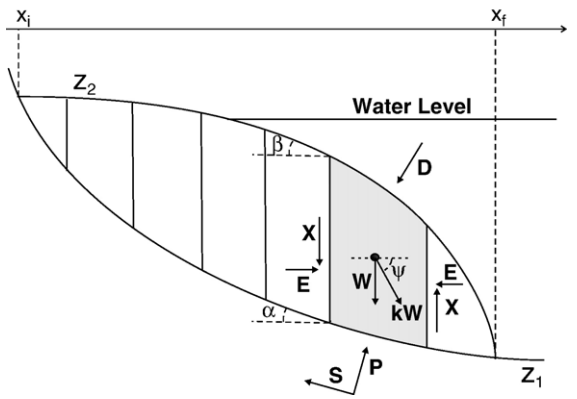


Fig. 6. Sketch of the vertical cross-section of the sliding body cut into slices, with representation of the forces acting on each single slice. All variables are defined in the text. Here W is the total weight of the slice and is given by the product of ψ times the slice horizontal length.

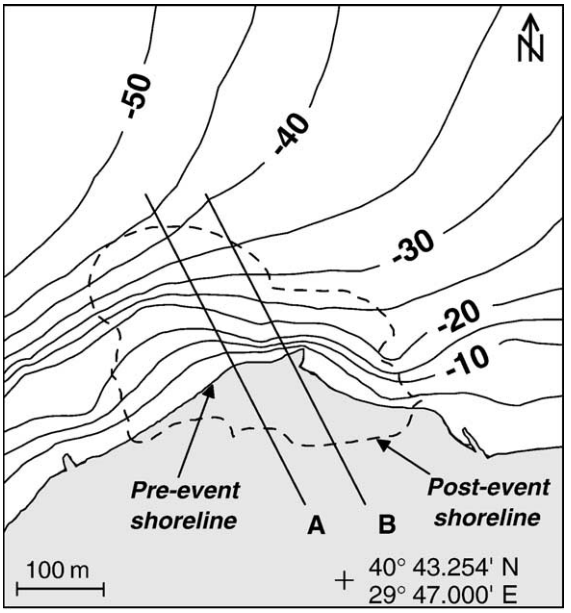


Fig. 7. Reconstruction of the pre- and post-slump coastline (Rathje et al., 2002, 2004; Cetin et al., 2004). The footprint of the failing mass (dashed line) and profiles A and B (solid lines) of the analysed vertical cross-sections are also shown.

magnitude of the inter-slice forces to the weight of the slide:

$$\delta = W^{-1}\left[\frac{1}{(x_f - x_i)}\int_{x_i}^{x_f}\left(E(x)^2 + X(x)^2\right)dx\right]^{1/2}$$

$$W = \int_{x_i}^{x_f} w dx$$

and by further adopting the principle of Minimum Lithostatic Deviation (MLD). It asserts that the state of limit equilibrium of the body is the state that satisfies all the five equations given above together with the six boundary conditions and that, in addition, minimises the lithostatic deviation $\delta$.

The new approach changes drastically the way the solution can be searched for. The stability factor is not treated as an unknown parameter anymore, but it is taken as a given parameter that can vary within a specified range including the critical value 1. The method we use consists in expressing the unknown function $X$ into a truncated Fourier expansion, and then to find the ensemble of exact solutions to the stability problem corresponding to any pre-given value of $F$. For each solution, the lithostatic deviation is computed, and, according to the MLD criterion, one picks up the value of $F$ that is associated with the solution corresponding to the minimum value of $\delta$ (Tinti and Manucci, in press).

To study the Değirmendere slump the TM method was applied together with various traditional limit equilibrium methods. We selected two profiles along the body that are aligned with the direction of sliding. These are given in Fig. 7 where the reconstructed footprint of the failing mass is portrayed. The two cross-sections, denoted by A and B, are taken along the average direction of sliding motion and are given in Fig. 8: the top curve has an average slope of about 15°. To perform the stability analysis the bottom boundary is approximated by an arc-like curve. Notice that this is not a requirement imposed by our approach, for it can be applied to slip boundaries with arbitrary shape, but rather it is a convention adopted by the traditional methods, and we adhere to it to allow comparison. We have studied the stability of the body in three different situations: in the pre-earthquake condition, during the shock, and also in the course of the first

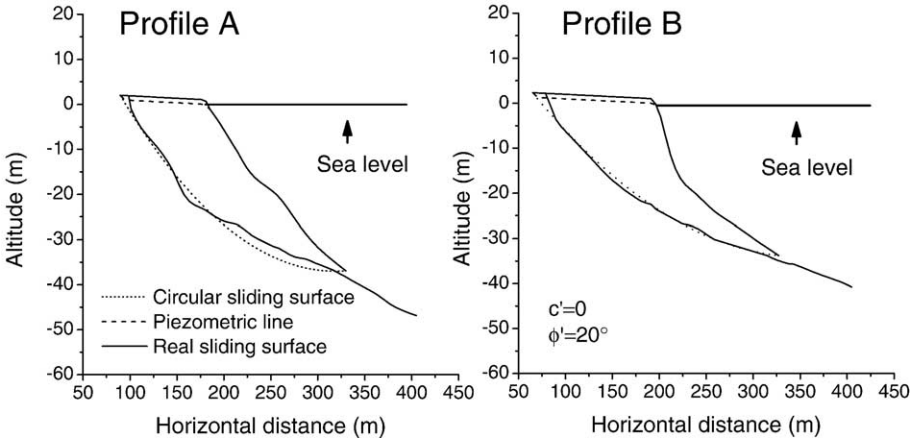


Fig. 8. Reconstructed vertical cross-sections of the slump body taken along transects A and B shown in Fig. 7. The assumed basal slip surface is circular and plotted as a dashed line. In the stability analysis the material is taken to be cohesionless ($c' = 0$) and with angle of friction $\phi' = 29°$.

Table 3
Safety factor $F$ and lithostatic deviation $\delta$ computed for the two body profiles A and B shown in Fig. 8 in the absence and in the presence of seismic load

| | Profile A, earthquake: $k=0.45$, $\psi=-22°$, tsunami: sl=−1 m | | Profile B, earthquake: $k=0.45$, $\psi=-21°$, tsunami: sl=−1 m | | Profile A, no earthquake, no tsunami | | Profile B, no earthquake, no tsunami | |
|---|---|---|---|---|---|---|---|---|
| | $F$ | $\delta$ | F | $\delta$ | F | $\delta$ | F | $\delta$ |
| Ordinary | 0.848 | – | 0.951 | – | 5.842 | – | 7.061 | – |
| Bishop | 0.903 | 0.1591 | 0.986 | 0.1578 | 5.963 | 0.0685 | 7.128 | 0.0528 |
| Janbu | 0.884 | 0.1559 | 0.989 | 0.1560 | 5.884 | 0.0681 | 7.076 | 0.0526 |
| Spencer | 0.908 | 0.1738 | 0.989 | 0.1714 | 5.963 | 0.0680 | 7.127 | 0.0525 |
| Morg and Price | 0.908 | 0.1746 | 0.989 | 0.1724 | 5.963 | 0.0679 | 7.127 | 0.0525 |
| Our method | 0.906 | 0.1620 | 0.989 | 0.1639 | 5.966 | 0.0672 | 7.115 | 0.0523 |

Observe that classical limit equilibrium methods and our approach provide quite similar results for this slope. The body is found to be very stable in pre-earthquake conditions ($k=0$), which is mainly due to the bottom friction and to the stabilising hydrostatic load of the sea. Conversely, $F$ collapses to critical values of instability in case of seismic load and tsunami attack: the seismic acceleration is taken as large as 0.45 g and the sea is assumed to be 1 m below the ordinary level, in consequence of the water retreat caused by the arriving tsunami. The value used for $\psi$ is the one that is found to produce the maximum instability. Notice that the methods given in the first three rows do not provide exact solutions to the stability equations, while Spencer's, Morgenstern and Price's and ours do.

arrival phase of the earthquake-induced tsunami. The results are summarised in Table 3 and in Fig. 9. Table 3 concerns both profiles A and B, and provides safety factors computed by applying traditional methods as well as our approach. The first observation is that the results happen to be quite similar, which helps us focus on the physics of the problem more than on algorithms. The pre-earthquake condition is a condition with no seismic load ($k=0$) and with normal sea level. The coastal slope results to be totally stable owing to the concurrent effects of the bottom friction and of the hydrostatic load exerted by the weight of the seawater column. In the problem formulation highlighted above, the seismic load is introduced by means of a static force that is applied to the centre of mass of each slice along the direction specified by the seismic angle $\psi$ that is measured clockwise from the horizontal axis. Consequently, $\psi=90°$ identifies a seismic force pointing vertically downward and $\psi=0°$ specifies a downslope horizontal force (see the sketch of Fig. 6). The magnitude of the force is given through the corresponding acceleration that is scaled to the gravity acceleration $g$

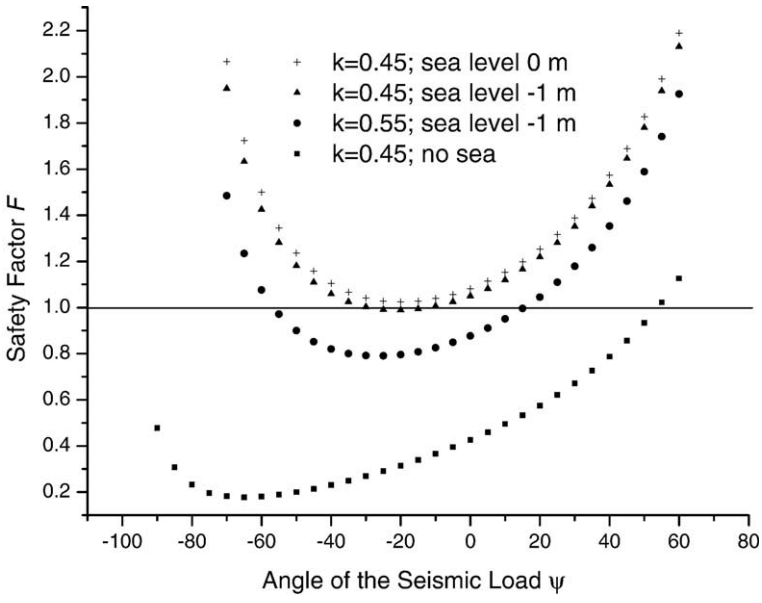


Fig. 9. Factor of safety vs. the orientation of the seismic force kW, expressed through the angle $\psi$ defined in Fig. 6.

by means of the factor $k$. In our computations we have assumed values for $k$ as large as 0.45 and 0.55, which are quite reasonable in view of the experimental data set of recorded peak ground accelerations (Barka et al., 2002; Cetin et al., 2004) and of acceleration modeling (Yagi and Kikuchi, 2000). The first arrival of the tsunami that was induced by the earthquake caused the sea to retreat from the usual shoreline almost along the entire coast of the İzmit bay, and Değirmendere was no exception. Hence, as regards the stability analysis, the condition of the tsunami attack is represented by lowering the sea level by 1 m, which implies a reduction of the hydrostatic load on the submarine slope.

Columns 1 and 2 of Table 3 show results of computations with both loads applied: calculations refer to the value of $\psi$ that is found to be the one producing the most unstable condition for a given profile. The dependence of $F$ from the angle $\psi$ is explored in detail in Fig. 9, where all computations are performed by means of our approach on the profile B. The various curves plotted here serve to show the effect of changing the hydrostatic and the seismic load on the resulting factor of safety. All curves are quite regular and display a well defined minimum, corresponding to negative values of $\psi$, and show that the most destabilising seismic load has both a downslope and an upward component. Increasing the seismic force magnitude from $k=0.45$ to $k=0.55$ reduces the safety factor by 0.1–0.2 and widens sensibly the interval of angles that may give rise to instability. Conversely, increasing the hydrostatic load has the effect of making the slope more stable. This is clearly seen by comparing the three curves corresponding to the same seismic load ($k=0.45$), but with different assumed value of water level. The case of no sea load is added in the figure only to prove that this term cannot be neglected in computing $F$, since this would lead to unacceptable underestimation. Observe that varying the water level by 1 m implies differences in the order of 0.05 in the resulting values of the factor of safety. These are not large, but are sufficient to support the idea that the tsunami may have contributed to destabilising the slope, though it could be hardly seen as the main cause of the failure.

## 7. Simulations of the slump and of the induced tsunami

Tsunami simulations showed a satisfactory agreement with real data, assuming the whole set of the strike- and dip-slip faults as the triggering cause, except in the Değirmendere area, where observations are greatly underestimated. In this section we investigate the motion of the slump and the characteristics of the generated tsunami, by means of a numerical simulation method that is based on a double simulation code, one for the slump and one for the tsunami.

The computation of the slump dynamics makes use of a numerical Lagrangian model that divides the slump into a 2D matrix of deformable blocks (24 in the present case) with quadrilateral basis and calculates the motion of each block taking into account all the relevant forces, namely gravity, buoyancy, the basal surface friction, the seawater drag on the frontal and upper body surfaces, as well as the interaction with the next neighbours (see Tinti et al., in press for a more detailed description). Fig. 10 displays the curves of the absolute value of the computed block velocities vs. time, as well as the speed of the slump centre of mass that is obtained as the weighted average of the blocks speed. Blocks move with rather different velocities in

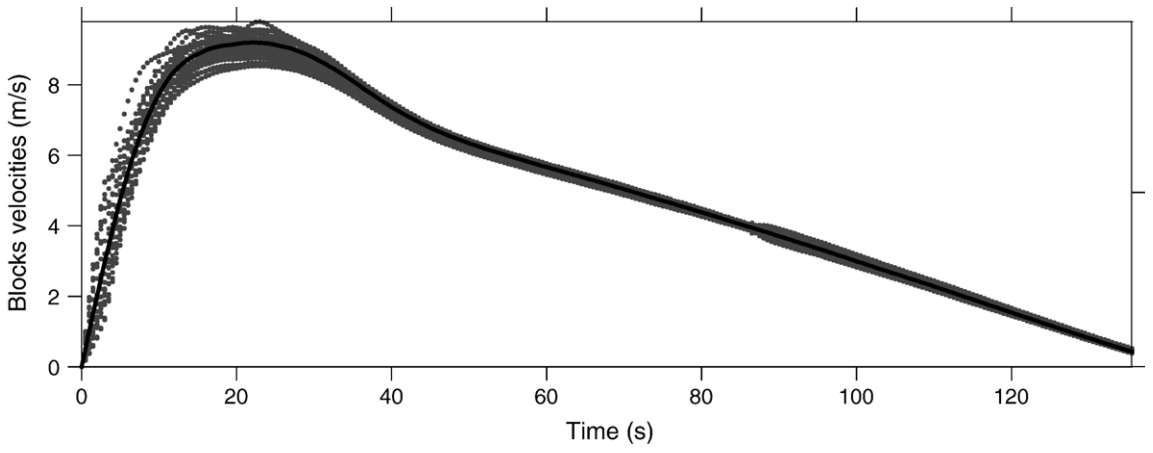


Fig. 10. Absolute value of the velocities of the blocks forming the slump vs. time. The mean velocity is plotted as a continuous black line.

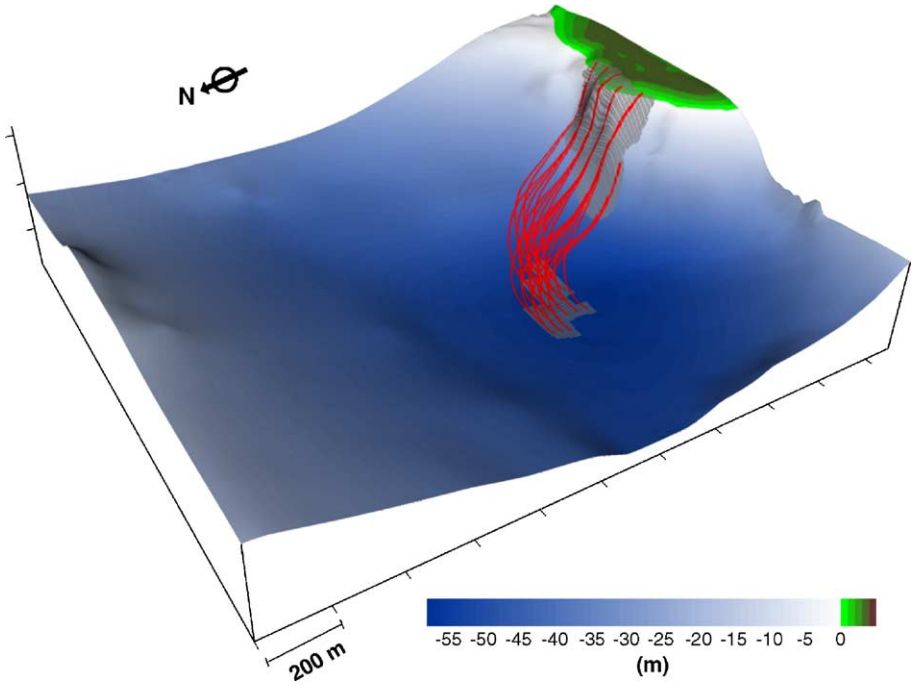


Fig. 11. 3D view of the trajectories of the 24 blocks forming the slide computed by means of the numerical model.

the initial phase of strong acceleration, and then, during the subsequent deceleration phase, they tend to move more uniformly, with the consequence that the entire mass advances almost like a rigid body. The slide is rather slow, attaining the maximum speed of about 9 m/s, and comes to a rest in slightly more than 2 min. Consequently, the computed run-out is short, about 500 m. The block trajectories, depicted in the 3D perspective of Fig. 11, run along the maximum bathymetric gradient (first northwestward and then westward), ending at about 45–50 m depth.

The induced tsunami is simulated through a shallow-water code based on the finite-element technique that solves the non-linear Navier-Stokes equations for inviscid incompressible fluid. The model accounts for the wave forcing due to the mass movement by means of an excitation term that depends on the rate of vertical displacement of the sea bottom $\partial_t h$, modified through a suitable filtering function depending on the local depth and on the lateral size of the slide. Here $h(x,y,t)=H(x,y)+H_s(x,y,t)$ represents the sea bottom as the sum of the time-independent bathymetry function

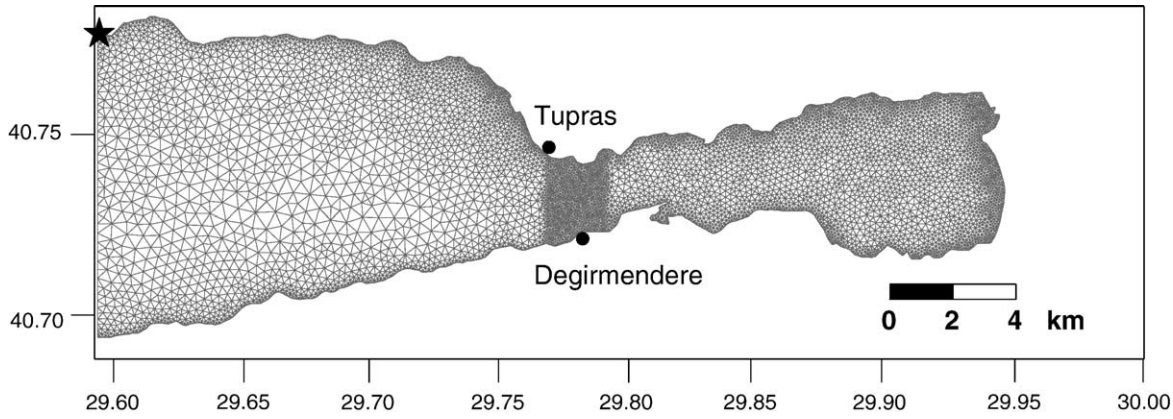


Fig. 12. Finer grid used in the slump-induced tsunami simulation. Notice that the grid has very high resolution in the Değirmendere-Tupras region where the tsunami is generated and propagates first.

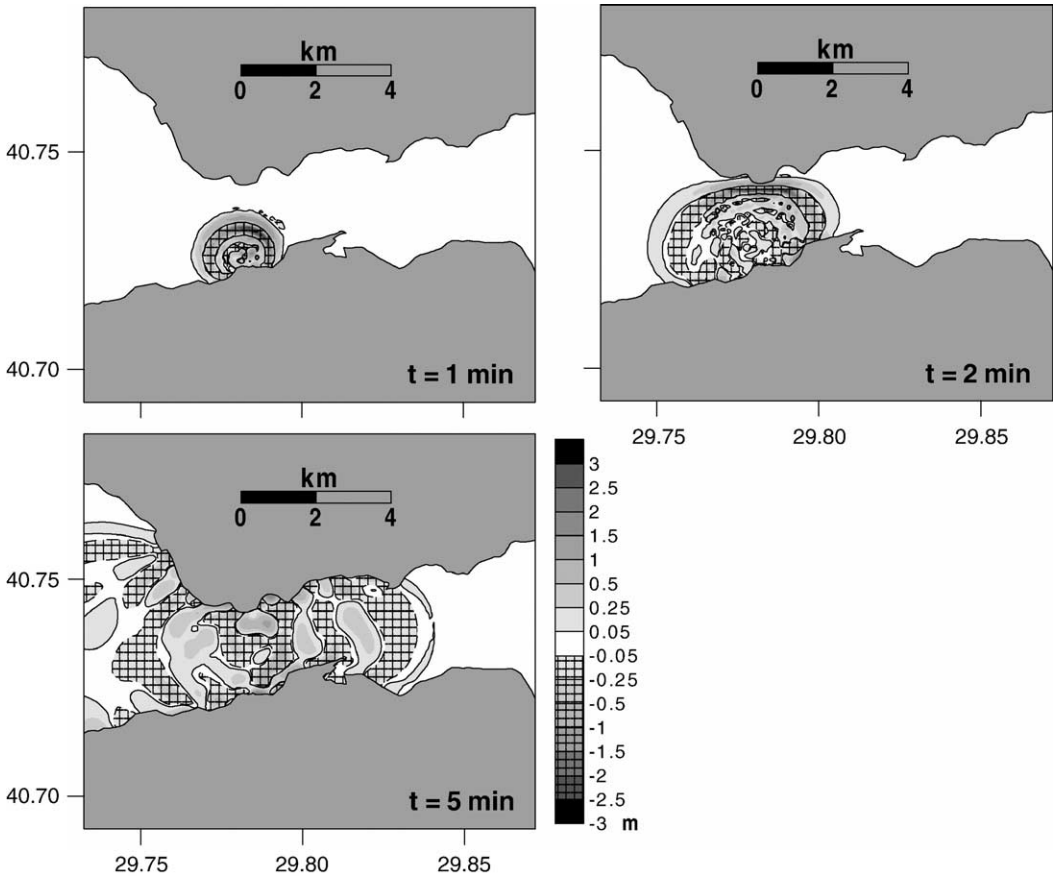


Fig. 13. Snapshots of the calculated water elevation fields in the source area at different times after the slide initiation.

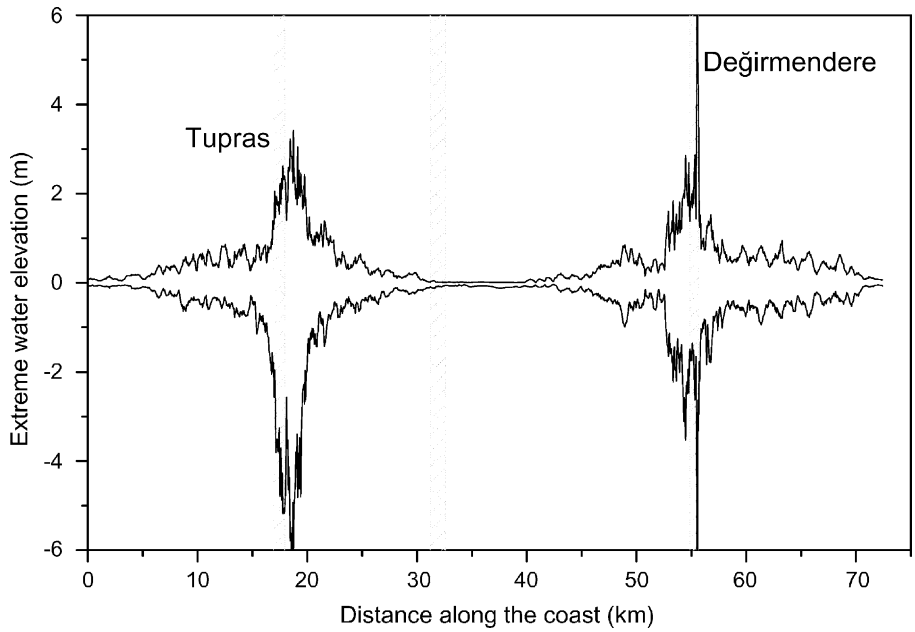


Fig. 14. Water maxima and minima along the coast. Observe the fast decay of the tsunami away from the source: f.i. see that in the İzmit area the tsunami is very weak. The distance is measured along the coast starting from the node that is in the northwestern corner of the grid of Fig. 12. We remark that the vertical peaks computed in Değirmendere go out of scale and exceed 8 m.

$H(x,y)$ and the landslide term $H_s(x,y,t)$, which is the instantaneous thickness of the body seen in the point $(x,y)$ at the time $t$. Further details on the model and on the filtering function are omitted here and may be found in previous papers addressing analogous problems of tsunamis induced by landslides (see Tinti et al., 1999, in press). The finite-element grid, consisting of 7451 nodes and 13,563 triangles, is built with high-resolution in the source region where the typical element size is less than 20 m, and covers the central and eastern part of the İzmit bay, as may be seen from Fig. 12. Snapshots of the tsunami wave field are portrayed in Fig. 13, from which we can notice how the wave propagates from Değirmendere and, after reaching the opposite coast, travels eastward (slower) and westward (faster) with different speeds owing to the different water depth of the basins. Fig. 14 displays the maxima and the minima of the water elevation computed in the coastal nodes. It can be seen that the tsunami is very strong at the source with a peak–peak height exceeding 12 m, but it drops drastically as soon as one moves some kilometers away. At Tupras, that is found on the opposite side of the bay, the maximum amplitude of the wave is around 3 m, and less for the other towns. Synthetic tide-gauge records for some grid nodes corresponding to Değirmendere and Tupras are shown in Fig. 15. Observe that in the source the waves are high-amplitude and short-period, with a clear sea retreat occurring first. The largest disastrous wave series, composed of a few (two–three) waves, attacks the Deðirmendere coast within the first minute and the wave energy is concentrated in a short time window less than 100 s. From Fig. 13 one learns that the tsunami arrives at the opposite coast in less than 2 min, and from the marigrams of Fig. 15 one sees that Tupras is reached soon after by longer period waves with a positive leading front.

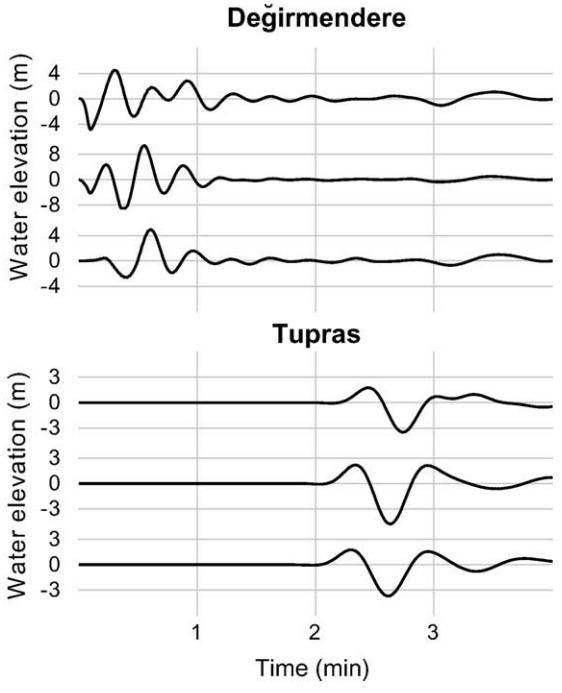


Fig. 15. Time histories computed in coastal nodes in the source region (Değirmendere) and in Tupras on the opposite coast of the bay.

## 8. Conclusions

The study conducted in this paper has shown that the tsunami that was observed in the İzmit bay in the night of August 17, 1999 can be explained only as the combined effect of several sources: tectonic coseismic displacements and local mass failure. One relevant result is that the sea bottom displacements computed by means of the classical elastic models, such as Okada's, from the set of the five right-lateral faults, that were the chief responsible for the disastrous seismic waves (see Table 2), are not sufficient to produce a sizeable tsunami. And this irrespective of the fact that the main rupture zone of the Kocaeli earthquake is or is not assumed to extend with an additional fault into the eastern part of the Marmara Sea, since the tsunamigenic contribution of the Marmara fault is negligible. In order to explain the main features of the regional tsunami affecting the İzmit bay, dip-slip faults have to be invoked capable to produce significant offset of the seafloor in the bay. In this paper we have assumed that such faults may be found in the system of normal faults that are associated with the step-over zones marking the transition from one strike-slip fault segment to the next (see Fig. 2). In particular, we have considered the graben-like fault systems in the central (Karamürsel) and eastern (İzmit) basins of the bay. The selected fault parameters match the idea that these are very shallow ancillary faults that contributed only marginally to the catastrophic seismic shaking of the main earthquake. They are however important enough to induce relevant vertical movement in the sea bottom. The computer simulation of the tsunami shows that only with the inclusion of these additional sources the run-up heights that were observed or assessed by the post-tsunami field surveys and that fall in the interval 1–3.5 m can be reproduced reasonably. The exception of Değirmendere that was attacked by waves several meters high according both to eyewitnesses and to post-event observations is due to a local slump. The stability analysis carried out on the basis of geotechnical data (defining the material property of the failing mass) and of bathymetric surveys

(capable of detailing the sliding surface and the run-out distance) shows that the body was mainly destabilised by the seismic load, but it also suggests that the tsunami may have had a triggering role. In fact the first manifestation of the regional tsunami was here, like in most other coastal segments, a sea withdrawal, and a sea level lowering with the corresponding decrease of hydrostatic load on the slope was shown to have the effect of decreasing the safety factor of the slide. The simulation of the slump motion was carried out by a suitable landslide evolution model that shows that the slump moves rather slow, attaining speed at most less than 10 m/s. The outcome of the slide model was used to compute the forcing term in the hydrodynamic equations governing the tsunami generation and propagation. Computer tsunami simulations via a finite-element model have shown that the slump generation mechanism is capable of producing very large short-period waves that are very local and match the tsunami observations in Değirmendere.

## Acknowledgements

The research has been funded partly by INGV (Istituto Nazionale di Geofisica e Vulcanologia, Rome, Italy) and partly by MIUR (Ministero dell'Istruzione, dell'Università e della Ricerca) to study tsunami generated by earthquakes and by underwater mass movements. This work was partly supported by the Research Fund University under the Project Number: UDP-328/03062004 allocated to Y. Altinok.

## References

Alpar, B., 1999. Underwater signatures of the Kocaeli earthquake (August 17th 1999). Turk. J. Mar. Sci. 5, 111–130.

Alpar, B., Yaltirak, C., 2002. Characteristic features of the North Anatolian Fault in the eastern Marmara Region and its tectonic evolution. Mar. Geol. 190, 329–350.

Altinok, Y., Ersoy, Ş., 2000. Tsunamis observed on and near the Turkish coast. Nat. Hazards 21, 185–205.

Altinok, Y., Alpar, B., Ersoy, Ş., Yalçiner, A.C., 1999. Tsunami generation of the Kocaeli Earthquake (August 17th 1999) in the İzmit Bay: coastal observations, bathymetry and seismic data. Turk. J. Mar. Sci. 5, 131–148.

Altinok, Y., Tinti, S., Alpar, B., Yalçiner, A.C., Ersoy, Ş., Bortolucci, E., Armigliato, A., 2001. The Tsunami of August 17, 1999 in İzmit Bay, Turkey. Nat. Hazards 24, 133–146.

Ambraseys, N.N., 1962. Data for the investigation of the seismic sea-waves in the Eastern Mediterranean. Bull. Seismol. Soc. Am. 52, 895–913.

Ambraseys, N.N., 2002a. The seismic activity of the Marmara Sea region in the last 2000 years. Bull. Seismol. Soc. Am. 92, 1–18.

Ambraseys, N.N., 2002b. Seismic sea-waves in the Marmara Sea region during the last 20 centuries. J. Seismol. 6, 571–578.

Ambraseys, N.N., Finkel, C.F., 1991. Long term seismicity of İstanbul and of the Marmara Sea region. Terra Nova 3, 527–539.

Ambraseys, N.N., Finkel, C.F., 1995. The Seismicity of Turkey and Adjacent Areas. A Historical Review 1500–1800. Eren Yayinlari, İstanbul. 240 pp.

Arel, E., Kiper, B., 2000. The coastal landslide occurred by August 17, 1999 earthquake at Degirmendere (Kocaeli). Proceedings of Coastal Engineering 3rd National Symposium, October 5–7, 2000. Çanakkale, Turkey, pp. 45–55. (in Turkish).

Armijo, R., Meyer, B., Hubert, A., Barka, A., 1999. Westward propagation of the North Anatolian fault into the Northern Aegean: timing and kinematics. Geology 27, 267–270.

Armijo, R., Meyer, B., Navarro, S., King, G., Barka, A., 2002. Asymmetric slip partitioning in the Sea of Marmara pull-apart: a clue to propagation processes of the North Anatolian Fault? Terra Nova 14, 80–86.

Barka, A., 1992. The North Anatolian fault zone. Ann. Tecton. VI, 164–195. (Suppl.).

Barka, A., Kadinsky-Cade, K., 1988. Strike-slip fault geometry in Turkey and its influence on earthquake activity. Tectonics 7, 663–684.

Barka, A., Akyüz, H.S., Cohen, H.A., Watchorn, F., 2000. Tectonic evolution of the Niksar and Tasova-Erbaa pull-apart basins, North Anatolian Fault Zone: their significance for the motion of the Anatolian block. Tectonophysics 322, 243–264.

Barka, A., Akyüz, H.S., Altunel, E., Sunal, G., Çakir, Z., Dikbas, A., Yerli, B., Armijo, R., Meyer, B., Chabaler, J.B, Rockwell, T., Hartleb, J., Dawson, T., Christofferson, S., Tucker, A., Fumal, T., Langridge, R., Stenner, H., Lettis, W., Bachhuber, J., Page, W., 2002. The surface rupture and slip distribution of the 17 August 1999 İzmit earthquake (M 7.4) North Anatolian Fault. Bull. Seismol. Soc. Am. 92, 43–60.

Çakir, Z., de Chabalier, J.B., Armijo, R., Meyer, B., Barka, A., Peltzer, G., 2003. Coseismic and early post-seismic slip associated with the 1999 İzmit earthquake (Turkey), from SAR interferometry and tectonic field observations. Geophys. J. Int. 155, 93–110.

Cetin, K.O., Isik, N., Unutmaz, B., 2004. Seismically induced landslide at Değirmendere Nose, İzmit bay during Kocaeli (İzmit)-Turkey earthquake. Soil Dyn. Earthqu. Eng. 24, 189–197.

Delouis, B., Giardini, D., Lundgren, P., Salichon, J., 2002. Joint inversion of InSAR, GPS, teleseismic, and strong-motion data for the spatial and temporal distribution of earthquake slip: Application to the 1999 İzmit mainshock. Bull. Seismol. Soc. Am. 92, 278–299.

Feigl, K.L., Sarti, F., Vadon, H., McClusky, S., Ergintav, S., Durand, P., Bürgmann, R., Rigo, A., Massonet, D., Reilinger, R., 2002. Estimating slip distribution for the İzmit mainshock from coseismic GPS, ERS-1, RADARSAT, and SPOT measurements. Bull. Seismol. Soc. Am. 92, 138–160.

Flerit, F., Armijo, R., King, G.C.P., Meyer, B., Barka, A., 2003. Slip partitioning in the Sea of Marmara pull-apart determined from GPS velocity vectors. Geophys. J. Int. 154, 1–7.

Gülen, L., Pinar, A., Kalafat, D., Ozel, N., Horasan, G., Yilmazer, M., Isikara, A.M., 2002. Surface fault breaks, aftershocks distribution, and rupture process of the 17 August 1999 İzmit, Turkey, earthquake. Bull. Seismol. Soc. Am. 92, 230–244.

Güneysu, A.C., 1999. The bathymetry of the İzmit bay. Turkish. J. Mar. Sci. 5, 167–169.

Hubert-Ferrari, A., Barka, A., Jacques, E., Nalbant, S.S., Meyer, B., Armijo, R., Tapponier, P., King, G.C.P., 2000. Seismic hazard in the Marmara Sea region following the 17 August 1999 İzmit earthquake. Nature 404, 269–273.

Hubert-Ferrari, A., Armijo, R., King, G., Meyer, B., Barka, A., 2002. Morphology, displacement, and slip rates along the North Anatolian Fault, Turkey. J. Geophys. Res. 107 (B10), 2235. doi:10.1029/2001JB000393.

Kuran, U., Yalçiner, A.C., 1993. Crack propagations earthquakes and tsunamis in the vicinity of Anatolia. In: Tinti, S. (Ed.), Tsunamis in the World. Kluwer Academic Publishers, pp. 159–175.

Kuşçu, İ., Okamura, M., Matsuoka, H., Awata, Y., 2002. Active faults in the gulf of İzmit on the North Anatolian fault, NW Turkey: a high resolution shallow seismic study. Mar. Geol. 190, 421–443.

Le Pichon, X., Şengör, A.M.C., Demirbağ, E., Ranging, C., İmren, C., Armijo, R., Görür, N., Çağatay, N., Mercier de Lepinay, B., Meyer, B., Saatçılar, R., Tok, B., 2001. The active main Marmara fault. Earth Planet. Sci. Lett. 192, 595–616.

Lettis, W., Bachhuber, J., Barka, A., Witter, R., Brankman, C., 2001. Surface fault rupture and segmentation during the Kocaeli earthquake. In: Barka, A., Kozaci, İ., Akyüz, S., Altunel, E. (Eds.), The 1999 İzmit and Düzce earthquakes: Preliminary Results. İstanbul Technical University, İstanbul, Turkey, ISBN: 975-561-182-7 pp. 31–54.

Lettis, W., Bachhuber, J., Witter, R., Brankman, C., Randolph, C.E., Barka, A., Page, W.D., Kaya, A., 2002. Influence of releasing step-overs on surface fault rupture and fault segmentation: examples from the 17 August 1999 İzmit earthquake on the North Anatolian Fault, Turkey. Bull. Seismol. Soc. Am. 92, 19–42.

Okada, Y., 1992. Internal deformation due to shear and tensile faults in a half-space. Bull. Seismol. Soc. Am. 82, 1018–1040.

Papadopoulos, G.A., 2001. Tsunamis in the Eastern Mediterranean: a catalogue for the area of Greece and adjacent seas. Proceedings of the Joint IOC–IUGG International Workshop: Tsunami Risk Assessment Beyond 2000: Theory, Practice and Plans, Moscow, Russia, June 14–16, 2000, pp. 34–43.

Parsons, T., 2004. Recalculated probability of $M \geq 7$ earthquakes beneath the Sea of Marmara, Turkey. J. Geophys. Res. 109 (B05304). doi:10.1029/2003JB002667.

Parsons, T., Toda, S., Stein, R.S., Barka, A., Dieterich, J., 2000. Heightened odds of large earthquakes near İstanbul: an interaction-based probability calculation. Science 288, 661–665.

Piatanesi, A., Tinti, S., 1998. A revision of the 1693 eastern Sicily earthquake and tsunami. J. Geophys. Res. 103, 2749–2758.

Piatanesi, A., Tinti, S., 2002. Numerical modeling of the September 8, 1905 Calabrian (southern Italy) tsunami. Geophys. J. Int. 150, 271–284.

Rathje, E.M., Wright, S.G., Bachhuber, J., 2002. Evaluation of integrated seismic hazards and ground failure in pull-apart basin during 1999 Kocaeli earthquake, Turkey. Report to United States Geological Survey, Earthquake Hazard Reduction Program (available online at: http://erp-web.er.usgs.gov/reports/annsum/vol43/pt/g0043.pdf).

Rathje, E.M., Karatas, I., Wright, S.G., Bachhuber, J., 2004. Coastal failures during the 1999 Kocaeli earthquake in Turkey. Soil Dyn. Earthqu. Eng. 24, 699–712.

Rothaus, R., Reinhardt, E., Noller, J., 2004. Regional considerations of coastline change, tsunami damage and recovery along the southern coast of the Bay of İzmit (The Kocaeli (Turkey) earthquake of 17 August 1999). Nat. Hazards 31, 233–252.

Şengör, A.M.C., Demirbağ, E., Tüysüz, E., Kurt, H., Görür, N., Kuşçu, İ., 1999. A preliminary note on the structure of the Gulf of İzmit: implications for the westerly prolongation of the North Anatolian fault. In: Karaka, M., Ural, D. (Eds.), ITU-IHAS International Conference on the Kocaeli Earthquake, 17 August 1999, ITU Publication, pp. 25–38.

Sucuoğlu, H., Gülkan, P., Bakır, B.S., Özcebe, G., Tankut, T., Yılmaz, Ç., Ersoy, U., Erberik, A., Akkar, S., Gür, T., 2000. Kocaeli and Düzce earthquakes: Engineering Report, Joint report of the Turkish Chamber of Civil Engineers and the Middle East Technical University, Ankara, 174 pp., (in Turkish).

Tinti, S., Armigliato, A., 2003. The use of scenarios to evaluate tsunami impact in South Italy. Mar. Geol. 199, 221–243.

Tinti, S., Bortolucci, E., 1999. Strategies of optimal grid generation for finite-element tsunami models. Proc. International Conference on Tsunamis, Paris, 26–28 May 1998, pp. 269–294.

Tinti, S., Manucci, A., in press. Gravitational stability computed through the limit equilibrium method revisited. Geophys. J. Int.

Tinti, S., Gavagni, I., Piatanesi, A., 1994. A finite-element numerical approach for modelling tsunamis. Ann. Geophys. 37, 1009–1026.

Tinti, S., Bortolucci, E., Armigliato, A., 1999. Numerical simulation of the landslide-induced tsunami of 1988 in Vulcano island, Italy. Bull. Volcanol. 61, 121–137.

Tinti, S., Pagnoni, G., Zaniboni, F., in press. The landslides and tsunamis of 30th December 2002 in Stromboli analysed through numerical simulations. Bull. Volcanol.

US Geological Survey, 2000. Implications for earthquake risk reduction in the United States from the Kokaeli, Turkey, earthquake of August 17, 1999. USGS Circular 1193, p. 65. Available online at: http://geology.cr.usgs.gov/pub/circulars/c1193/index.html.

Yagi, Y., Kikuchi, M., 2000. Source rupture process of the Kocaeli, Turkey, earthquake of August 17, 1999, obtained by joint inversion of near-field data and teleseismic data. Geophys. Res. Lett. 27, 1969–1972.

Yalçiner, A.C., Altinok, Y., Synolakis, C.E., 2000. Tsunami Waves in İzmit Bay after the Kocaeli Earthquake. Earthquake Spectra, Kocaeli, Turkey Earthquake of August 17, 1999 Reconnaissance Report, Special Issue Supplement to Professional Journal of Earthquake Engineering Research Institute vol. 16, pp. 55–62.

Yalçiner, A.C., Imamura, F., Kuran, U., Çakiroğlu, Y., Özbay, I., Erdinç, E., Durmuşoğlu, Ö., Altinok, Y., Alpar, B., 2001a. An integrated model on the generation and propagation of tsunamis in the surrounding seas around Anatolia, Türkiye çevresi denizlerde tsunami dalgasi hareketi için bileşik model oluşturulmasi, . Final Report of Basic Research Project No: TUBITAK-YDABÇAG-60, November 2001, pp. 147 (in Turkish).

Yalçiner, A.C., Kuran, U., Altinok, Y., Alpar, B., Ersoy, Ş., 2001b. Historical earthquakes and associated tsunamis in the Aegean Sea, Türkiye kiyilarinda tarihsel depremler ve onlara ilişkin tsunamlerin izlerinin araştirilmasi. Final Report of Basic Research Project No: TUBITAK-INTAG-827, September 2001, pp. 74 (in Turkish).

Yalçiner, A.C., Synolakis, C.E., Alpar, B., Borrero, J., Altinok, Y., Imamura, F., Tinti, S., Ersoy, Ş., Kuran, U., Pamukçu, S., Kanoğlu, U., 2001c. Field surveys and modeling of the 1999 İzmit Tsunami. Proceedings of the International Tsunami Symposium, August 7–10, 2001, Seattle, Washington, USA, pp. 557–564.

Yalçiner, A.C., Alpar, B., Altinok, Y., Özbay, İ., Imamura, F., 2002. Tsunami in the sea of Marmara, historical documents for the past, models for the future. Mar. Geol. 190, 445–463.

Yalçiner, A.C., Pelinovsky, E., Talipova, T., Kurkin, A., Kozelkov, A., Zaitsev, A., 2004. Tsunamis in the Black sea: comparison of the historical, instrumental and numerical data. J. Geophys. Res. 109, C12023. doi:10.1029/2003JC002113.

Yüksel, Y., Alpar, B., Yalçiner, A.C., Çevik, E., Ozgüven, O., Çelikoğlu, Y., 2002. Effects of the eastern Marmara Earthquake on marine structures and coastal areas. Water Marit. Eng. 156, 147–163.